Journal of the Iranian Chemical Society (2018) 15:1467–1475
https://doi.org/10.1007/s13738-018-1344-9

ORIGINAL PAPER

# Enhanced antibacterial activity of functionalized graphene by azo-pyridinium compounds

**Sakineh Omidi[1] · Ali Kakanejadifard[1] · Farideh Azarbani[2]**

Received: 23 December 2017 / Accepted: 12 March 2018 / Published online: 19 March 2018


## Abstract

For enhancement of antibacterial properties, two azo compounds were grafted on the aminated graphene by using the imine linkage. The azo compounds included pyridinium unit with different alkyl long chains. The new nanohybrids were characterized by Fourier transform infrared spectra, X-ray powder diffraction, ultraviolet–visible, field emission scanning electron microscopy (FE-SEM), atomic force microscopy, zeta potential, and energy-dispersive X-ray spectroscopy. The hybrids were investigated for antibacterial effect against *Staphylococcus aureus* and *Escherichia coli* as models of Gram-positive and Gram-negative bacteria. The nanohybrids showed a significant effect on both bacteria. Destruction of the cell wall and discharge of intracellular contents could be detected from FE-SEM images of bacteria after exposed to nanohybrids. The nanohybrid with $C_{10}$ alkyl chain in the pyridinium unit displayed the highest antibacterial activity.

## Graphical Abstract

Antibacterial activity of graphene–azo nanocomposite against *E. coli* and *S. aureus* was enhanced. Destruction of the cell wall and shrinking of bacteria are observed in FE-SEM image.

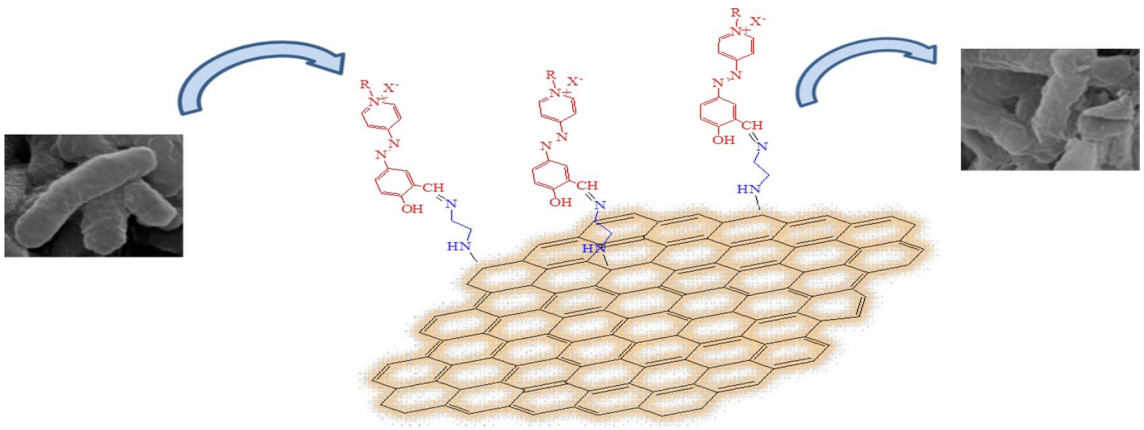

**Keywords** Antibacterial activity · Graphene · Imine linkage · Pyridinium salt

## Introduction

Graphene, a sheet of two-dimensional carbon framework, has attracted attention because of its specific surface area and excellent physical and chemical properties [1, 2]. Graphene's unique properties make it suitable for use in a variety of applications including nanoelectronic devices, transparent conductors, and nanocomposite materials [3–5].

✉ Ali Kakanejadifard
ali.kakanejadifard@gmail.com; kakanejadi.a@lu.ac.ir

[1] Department of Chemistry, Lorestan University, Khorramabad, Iran

[2] Department of Biology, Lorestan University, Khorramabad, Iran

Apart from these applications of graphene, it is drawing significant attention for biomedical uses such as delivery of genes and anticancer drugs [6, 7], nanosensors [8], and antibacterial applications [9–11]. The covalent functionalization of graphene oxide (GO), an oxidized derivative of graphene, with organic molecules is a methodology to make multifunctional agents. The hybrid may display the properties of both GO and the organic molecule. In recent years, several cases of noncovalent and covalent bonding of azo compounds to graphene-based materials have been reported. The noncovalent bondings are included in the assembly via electrostatic interactions [12], physisorbed directly onto graphene surface [13] or $\pi$–$\pi$ stacking through graphene outer face [14]. Graphene may also be adsorbed on an azobenzene self-assembled monolayer [15]. Covalent interaction of azo compounds through an ester [16] or amide linkage [17] has also been reported. However, azo-functionalization of graphene via imine linkages has not been investigated.

With growing concerns of microbial agents, there is a rising interest in the development of effective antibacterial products [18, 19]. A class of antibacterial materials is quaternary ammonium compounds (QACs) with general formula $R_4N^+X^-$. The fields of application of QACs are numerous [20, 21]. But one common problem in the case of QACs is the development of bacterial resistance [22]. An effective method to the progress of new routes to circumvent the bacterial resistance may be the conjugation of QACs with substrates (such as graphene-based materials) to improve the antibacterial activities of the obtained hybrid.

Herein we report the formation of a new graphene–azo hybrid through an imine linkage. The nanohybrids of graphene–azo were examined for antibacterial properties against Gram-positive (*Staphylococcus aureus*) and Gram-negative bacteria (*Escherichia coli*) bacteria. Obtained images from field emission scanning electron microscopy (FE-SEM) were used for the exhibition of changes in bacterial morphology.

## Experimental

### Materials and methods

All solvents and chemical reagents were purchased from Merck and Sigma-Aldrich companies. The solvents used in the reactions were of analytically reagent grade. For UV–Vis experiments the purity-grade solvents (> 99.9%) were used without any additional purification. 2-Hydroxy-5-(pyridine-4-yldiazenyl) benzaldehyde (AZO) has been synthesized and purified according to the method reported in the literature [23]. Azo-pyridinium compounds, AZO10 and AZO12, were synthesized by reaction of AZO with 1-Bromodecane and 1-Bromododecane, respectively. GO was synthesized according to an improved method from purified graphite [24].

#### Synthesis of aminated graphene oxide (GN)

Aminated graphene (GN) was prepared from GO according to the method reported, with a few modifications [25, 26]. In a typical experiment, 0.5 g GO was spread in 50 mL 1-butanol and sonicated for 60 min to give a uniform brown colloidal solution. The dispersed solution was added slowly over a period of 2 h to 10 mL of ethylenediamine (EDA). The excess EDA prevents cross-linking of graphene sheets. The mixture was heated and stirred for 8 h in 80–85 °C, then cooled down to room temperature, and centrifuged (6000 rpm for 10 min), and it was decanted. The residual solid material was washed with ethanol and centrifuged again (two times). The resultant solid was dried at room temperature

#### Preparation of nanohybrid of GN with AZO10 and AZO12 (GN-A10 and GN-A12)

In 50 mL *N*, *N*′-dimethylformamide (DMF) 200 mg GN was dispersed and sonicated for 30 min to get a homogeneous solution. Then 200 mg azo compound in 10 mL DMF and 0.5 mL formic acid was added to GN solution. The mixture was stirred at 70 °C for 36 h. The resultant GN-AZO hybrid was centrifuged, and the supernatant was decanted and rinsed with methanol until the supernatant became colorless (5–6 times). The attained solid was dried at room temperature.

#### Cell viability test and characterization of bacterial morphology

Antibacterial properties were evaluated by the colony counting method described in the literature [27]. FE-SEM images of bacteria were obtained by fixing the treated bacteria with 2.5% glutaraldehyde according to method described in the literature [27].

### Instruments

FT-IR spectra were registered on a Shimadzu 8400S spectrometer using KBr disk. The UV–Vis spectra were recorded with a Shimadzu 1650 spectrophotometer. Patterns of X-ray diffraction of the materials were recorded by a Halland Philips X-ray powder diffraction (XRD) diffractometer at a scanning speed of 2°/min from 10° to 100 (Cuk, radiation, $\lambda = 0.154056$ nm). Structure and morphology of nanomaterials were carried out using an LEO 440i Scanning Electron Microscope under vacuum at an operating voltage of 10 kV. Energy-dispersive X-ray microanalysis (EDX) system was

used to discover corresponding elements atomic numbers. Zeta potential measurements and atomic force microscopy (AFM) were carried out using a Nanotrac wave II Q Particle Size Analyzer equipped with a diode laser operating at 780.0 nm and AFM full plus model, respectively.

## Results and discussion

Azo-pyridinium compounds (AZO10 and AZO12) were synthesized according to the route shown in Fig. 1.

The functionalization of graphene with azo compounds is first initiated with amination of GO with ethylenediamine; the reaction of the aminated GO (GN) is then followed with related azo compounds. The complete synthesis process is shown in Fig. 2. The nanohybrids of GN with AZO10 and AZO12 are abbreviated as GN-A10 and GN-A12, respectively.

## Characterization

Figure 3 displays the FT-IR spectra of GO, GN, AZO10, and GN-A10 solid samples. The FT-IR spectrum of GO showed

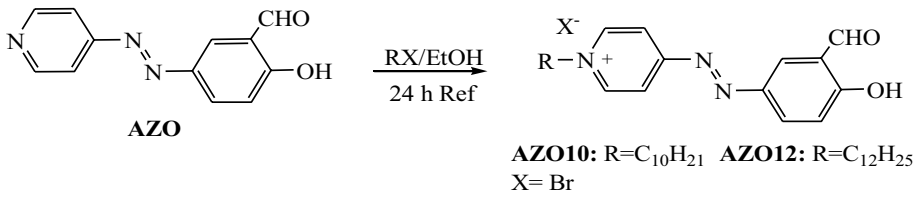


**Fig. 1** Synthesis of AZO10 and AZO12

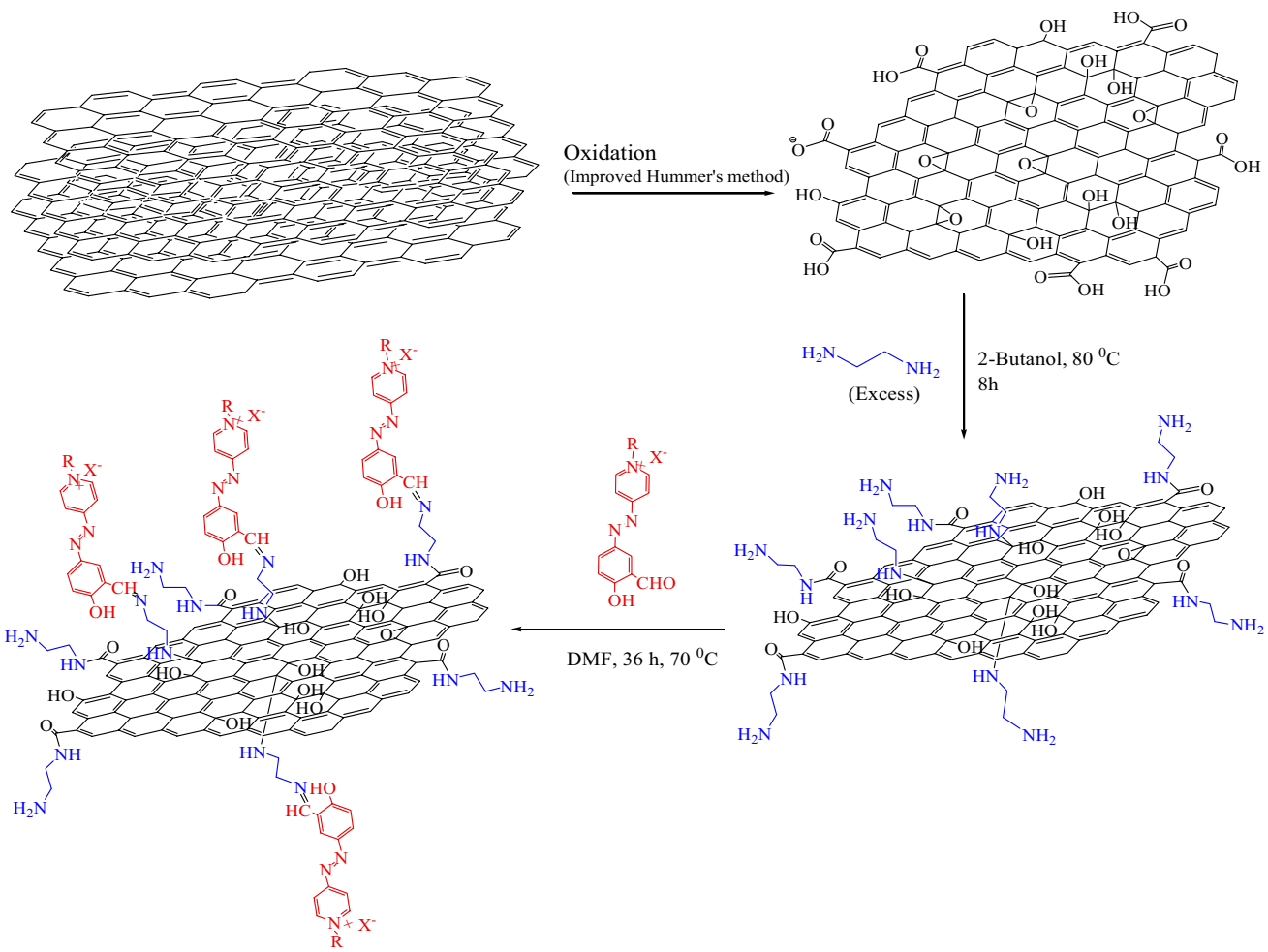


**Fig. 2** Synthesis route of GN-A10 and GN-A12

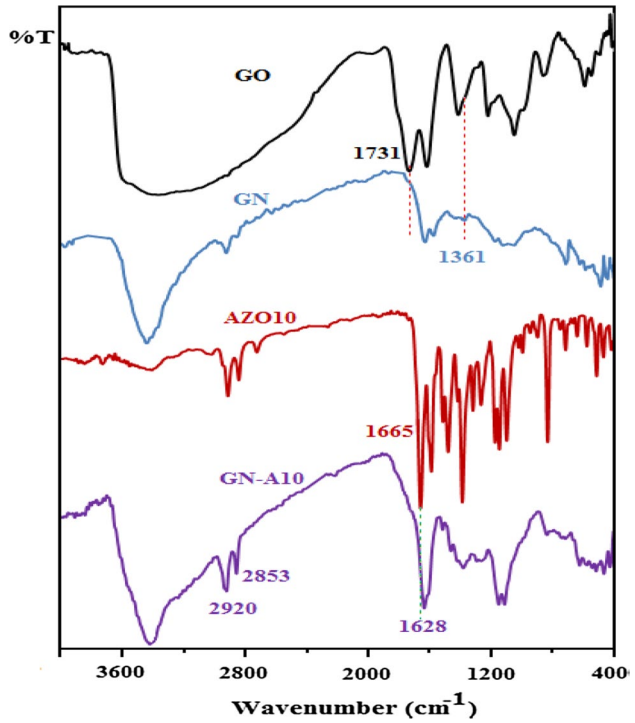


**Fig. 3** FT-IR spectra of GO, GN, AZO10, and GN-A10

the bands of hydrogen-bonded O–H (3100–3600 $cm^{-1}$), C=O (1731 $cm^{-1}$), C=C (1623 $cm^{-1}$), and C–O (1222, 1053 $cm^{-1}$). In GN spectrum a significant drop in strength of the band at 1731 $cm^{-1}$ was identified compared to original GO. The occurrence of two new bands at 1635 $cm^{-1}$(C=O of the amide bond) and 1361 $cm^{-1}$ (C–N) in the spectrum of GN indicates the complete grafting of EDA on the GO surface [25]. IR spectrum of AZO10 showed the absorption bands at 3360 $cm^{-1}$ (phenolic O–H), 2922 $cm^{-1}$ and 2853 $cm^{-1}$ (–$CH_2$ and –$CH_3$), 1665 $cm^{-1}$ (C=O), 1593 $cm^{-1}$ (N=N), 1390 $cm^{-1}$ (C–N), and 1102 $cm^{-1}$ (C–O). In the IR spectrum of GN-A10, the presence of new absorptions at 2853–2920 $cm^{-1}$ (aliphatic C–H) and 1599 $cm^{-1}$ for (N=N) indicates the formation of GN-A10. This spectrum also showed the absorption bands at 3400 $cm^{-1}$ (O–H), 1628 $cm^{-1}$ (C=N along with C=O of amide), 1375 $cm^{-1}$ (C–N), 1145 $cm^{-1}$, and 1107 $cm^{-1}$(C–O).

Kaiser ninhydrin test was performed to detect primary amine groups in the synthesized samples [28]. Based on this method, ninhydrin addition changes the color of aminated compounds to blue, while it has no effect on non-aminated compounds. Therefore, two individual tubes were considered and 1 mg GN or GN-A10 and a few drops of ninhydrin were added to each tube. The observed colors are depicted in Fig. 4. As Fig. 4a presents, the blue color signifies successful modification of GO by EDA. However, observation of the pale blue color in Fig. 4b implies that some unreacted amine groups exist at the surface of GN-A10.

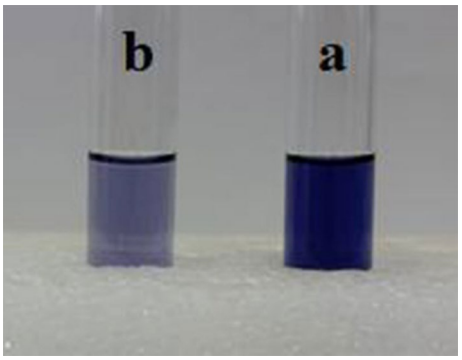


**Fig. 4** Ninhydrin test for 1 mg of **a** GN and **b** GN-A10

Figure 5a illustrates the XRD patterns of the GO and GN-A10 sample over the range of 10°–80°. The typical 2$\theta$ peak of GO at 10.74° matches (0 0 1) inter-planar spacing of 0.822 nm. For GN-A10, the (0 0 1) peak is absent, while two broad peaks arise at 2$\theta$ = 25.4° and 43.3°, attributing to the d-spacing of 0.35 and 0.21 nm, respectively, which correlated to the (0 0 2) and (1 0 0) peaks of graphite [29, 30]. The existence of electrostatic repulsion between the sheets in GO owing to the negatively charged carboxyl groups has been reported [31]. Due to the covalent functionalization, the electrostatic repulsion between sheets decreases and the aggregation of the sheets of GN has a strong impact on the crystal structure.

Since azo compounds have the characteristic absorbance in the UV–Vis light region (300–650 nm), the UV–Vis experiment was used to evaluate the formation of GN-A10. Figure 5b shows the UV–Vis spectra of AZO10 and GN-A10. The AZO10 shows a band at 248 nm attributed to the $\pi \rightarrow \pi^*$ transitions in the backbone of the aromatic ring and a second band located at 366 nm assigned to $\pi \rightarrow \pi^*$ due to the electronic transition of azo–aromatic chromophore [32, 33]. The grafting of AZO10 on GO was manifest from the spectrum of the GN-A10 solution, which indicates the individual absorption bands of AZO10 at 259 nm attributed to $\pi \rightarrow \pi^*$ transition of aromatic rings and at 365 nm attributed to $\pi \rightarrow \pi^*$ transition of the azo derivative.

The morphologies of GO and GN-A10 were detected by field emission scanning electron microscopy (FE-SEM). Figure 6a displays the FE-SEM image of the monolayer of graphene oxide with a smooth surface and some overlapping. Figure 6b, c shows the FE-SEM image of GN-A10 in two different magnifications at 1 µm and 500 nm. It shows that graphene sheets in the nanohybrid material are much wrinkled compared to the pristine GO. The reason can be attributed to chemical functionalization of the nanosheet material and aggregation of smaller flakes.

AFM was used to assess the changes in thickness of the nanohybrids. Figure 7a shows that the average thickness of GO is about 1.1 nm, while grafting EDA on GO sheets increases GO's thickness to about 2.8 nm. Functionalization

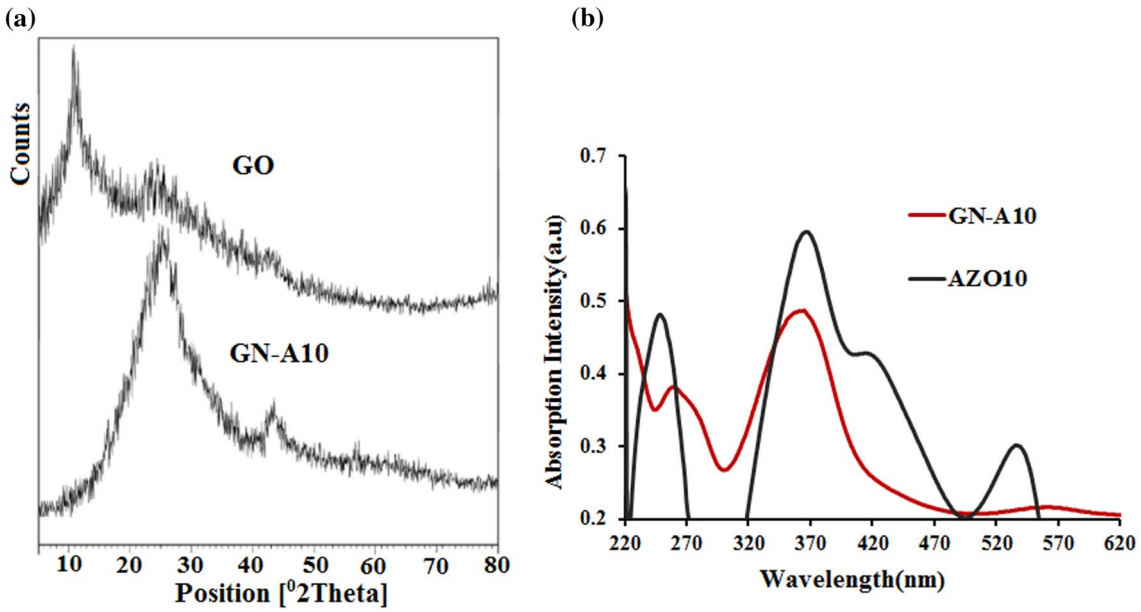


**Fig. 5** **a** XRD patterns of GO and GN-A10; (**b**) UV–Vis spectra of methanol solutions of AZO10 and GN-A10

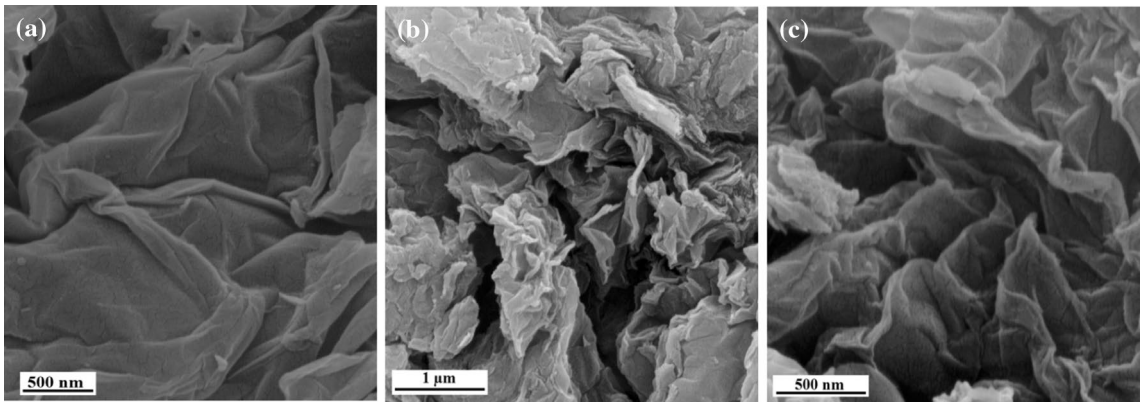


**Fig. 6** FE-SEM of **a** GO, and **b**, **c** GN-A10

of GN by azo compounds resulted in an increased thickness of about 28 nm (Fig. 7c). This is in agreement with the XRD and FE-SEM findings indicating GO sheets tend to aggregate after the functionalization by azo compounds. This phenomenon has also been observed in azo-functionalization of graphene by other methods [17].

Also, EDX results in Fig. 8a show that GN-A10 consists of four elements (C, O, N, and Br). The elemental maps of C, O, N, and Br GN-A10 nanohybrid are shown in Fig. 8b. The high content of nitrogen is owing to the existence of EDA and azo compounds on the surface of graphene. The presence of bromine verified that GN is functionalized with azo compounds even though the weight percentage of Br in the structure of GN-A10 is low. Therefore, the results unravel that the GN aggregates are cationic in nature. The zeta potential data showed that surface charge of GN-A10 is 52.6 mV that confirmed high functionalization of graphene with azo-pyridinium compounds.

## Antibacterial activity

Gram-negative *E. coli* (PTCC 1330) and Gram-positive *S. aureus* (PTCC 1112) were selected as two common model bacteria for tests of the antibacterial effects of nanohybrids. The photographs of antibacterial test are shown in Fig. 9. The viability of *E. coli* cells reduced 45.2, 84.8, and 74.4%, and the viability of *S. aureus* cells reduced 46.4, 90.3, and 82.5%, after incubating with GO, GN-A10, and GN-A12 aqueous suspensions, respectively (Fig. 10).

As shown in Fig. 10, the antibacterial activity of both GN-A10 and GN-A12 is higher than the antibacterial

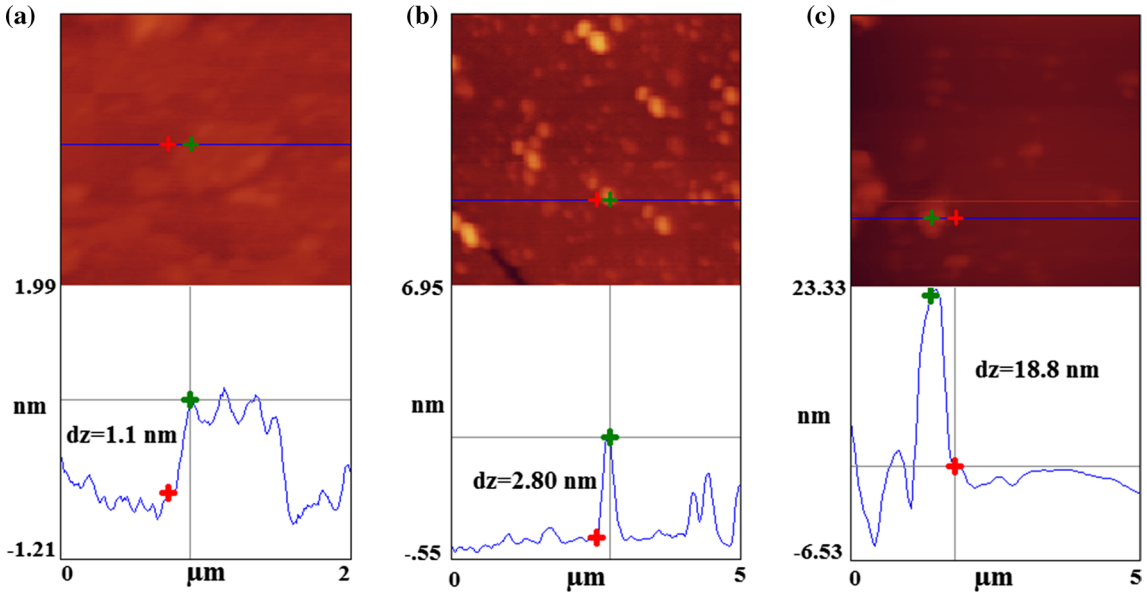


**Fig. 7** AFM images of **a** GO, **b** GN, and **c** GN-A10

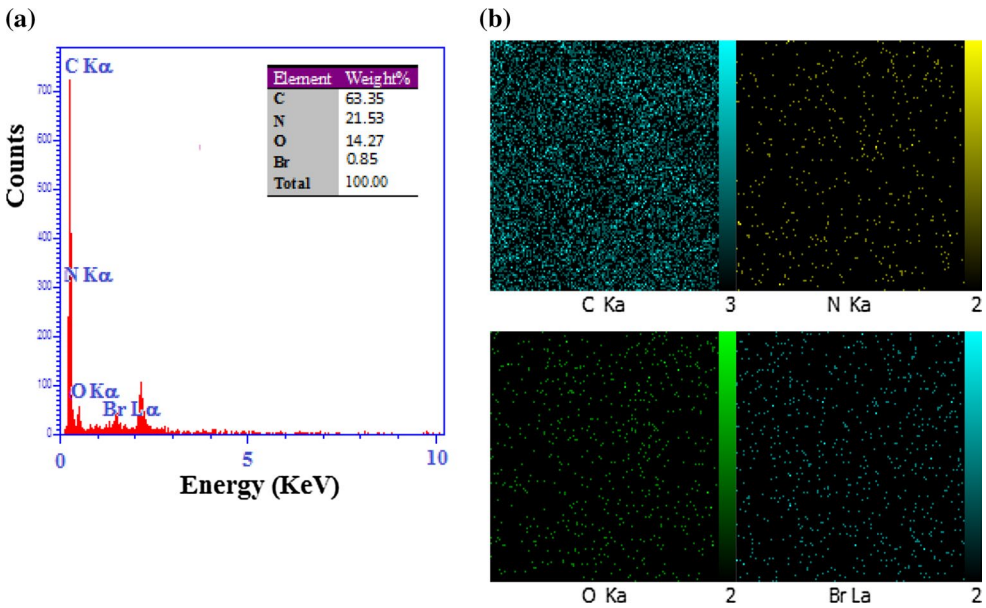


**Fig. 8** **a** EDX spectrograms and **b** elemental maps of GN-A10

performance of pure GO. The results showed that alkyl chains in the structure of nanohybrids affected their antibacterial activity. GN-A10 with $C_{10}$ alkyl chain in azo unit shows higher antibacterial activity relative to GN-A12. Also the antibacterial effect of nanohybrids against *S. aureus* was higher than that against *E. coli* bacteria. Gram-negative bacteria have an outer membrane that plays as a barrier to foreign factors. Therefore, the nanohybrids showed lower antibacterial activity toward Gram-negative (*E. coli*) bacteria. In general, the graphene-based material toxicity against bacteria is due to physical disruption as a result of direct contact with nanosheets of graphene or oxidative stress [27, 34, 35]. Since the bacterial cellular membrane bears negative charges and the quaternary ammonium compounds possess positively charged heads, they can interact with each other through electrostatic attraction. This electrostatic interaction is followed by penetration of the alkyl chains into the interface area, leading to disorganizing bacterial bilayer membranes and discharge of the cellular content [36]. FE-SEM images of *E. coli* and *S. aureus* before and after GN-A10 exposure were recorded to display changes in bacterial morphology.

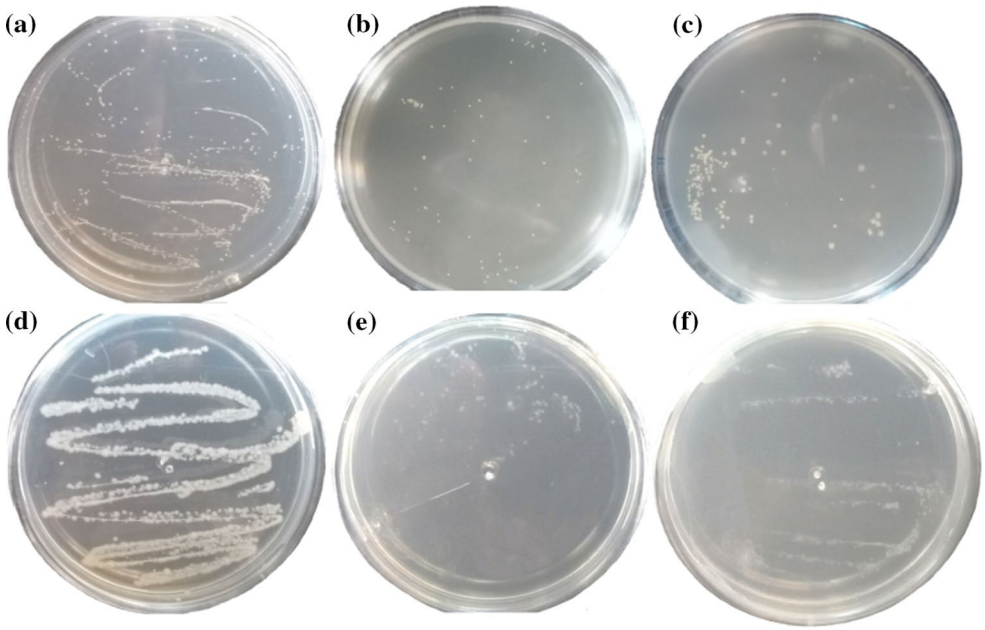


**Fig. 9** Photographic images of forming colonies: **a** control solution of *S. aureus* bacteria, **b** solution of *S. aureus* bacteria treated with 40 μg $mL^{-1}$ of GN-A10, **c** solution of *S. aureus* bacteria treated with 40 μg $mL^{-1}$ of GN-A12, **d** control solution of *E. coli* bacteria, **e** solution of *E. coli* bacteria treated with 40 μg $mL^{-1}$ of GN-A10, and **f** solution of *E. coli* bacteria treated with 40 μg $mL^{-1}$ of GN-A12

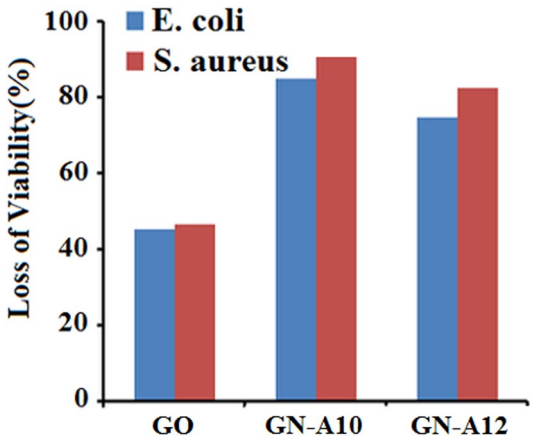


**Fig. 10** Viability of *E. coli* cells ($10^6$–$10^7$ CFU $mL^{-1}$) and *S. aureus* cells ($10^6$–$10^7$ CFU $mL^{-1}$) incubated with graphene-based materials suspensions (40 μg $mL^{-1}$) for 2 h

Figure 11b shows the cell morphology of *E. coli*. The interaction of GN-A10 sheets with bacterial surface leads to the destruction of the outer membrane causing discharge of cell content and bacterium death. The damage of the cell wall and shrinking of *S. aureus* bacteria are also observed (Fig. 11d).

According to the above discussion and FE-SEM images, it can be concluded that diffusion of alkyl chain of pyridinium unit into the injured bacteria membrane by graphene sheets is the key factor for antibacterial action of nanohybrids.

## Conclusion

In summary, two azo compounds with pyridinium unit were synthesized and grafted onto the surface of aminated graphene by imine linkage. FT-IR, UV–Vis, XRD, zeta potential, FE-SEM, AFM, and EDX spectroscopy confirmed the formation of new nanohybrids. XRD patterns, FE-SEM, and AFM analyses showed that aggregation of graphene sheets happens after hybridization with azo compounds. Antibacterial test revealed that nanohybrids exhibited good antibacterial action against *E. coli* and *S. aureus* bacteria. The treated bacteria were observed by FE-SEM images. The key factors including adsorption of bacteria onto the positively charged nanohybrids, destruction of cell wall bacteria in effect of direct contact with graphene nanosheets, and diffusion of alkyl chain of pyridinium unit into the injured membrane of bacteria are effective in the antibacterial activity. The obtained results by this work indicated that the modification of graphene-based material with other antibacterial compounds (such as QACs) can lead to a synergic effect in new nanohybrids material.

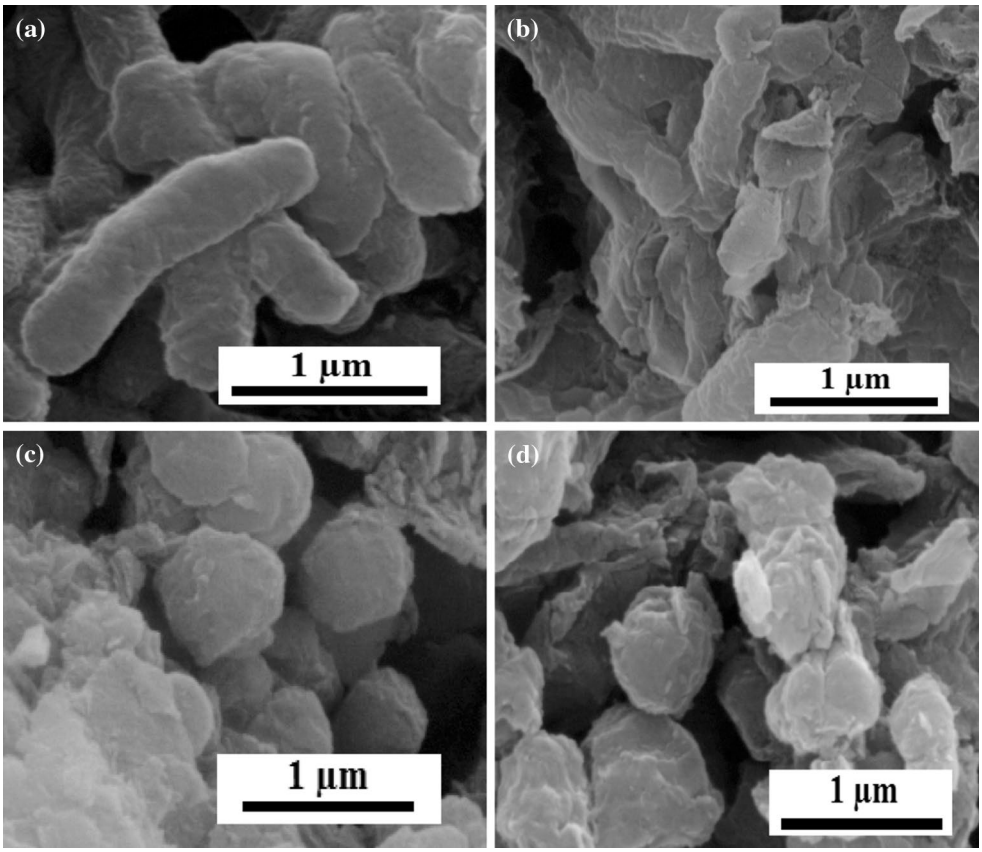


**Fig. 11** **a** SEM images of *E. coli* after incubation with saline solution for 2 h without graphene-based materials, **b** *E. coli* cells after incubation with GN-A10 dispersion (40 µg $mL^{-1}$) for 2 h, **c** *S. aureus* after incubation with saline solution for 2 h without graphene-based materials, and **d** *S. aureus* cells after incubation with GN-A10 dispersion (40 µg $mL^{-1}$) for 2 h

**Acknowledgements** We are grateful to the Lorestan University for financial support of this work.

## References

1. A.K. Geim, K.S. Novoselov, Nat. Mater. **6**, 183 (2007)
2. D. Li, R.B. Kaner, Nat. Nanotechnol. **3**, 101 (2008)
3. S. Watcharotone, D.A. Dikin, S. Stankovich, R. Piner, I. Jung, G.H. Dommett, G. Evmenenko, S.-E. Wu, S.-F. Chen, C.-P. Liu, Nano Lett. **7**, 1888 (2007)
4. H.A. Becerril, J. Mao, Z. Liu, R.M. Stoltenberg, Z. Bao, Y. Chen, ACS Nano **2**, 463 (2008)
5. R. Pasricha, S. Gupta, A.K. Srivastava, Small **5**, 2253 (2009)
6. M. Kim, N.S. Safron, C. Huang, M.S. Arnold, P. Gopalan, Nano Lett. **12**, 182 (2011)
7. X. Hu, D. Li, H. Tan, C. Pan, X. Chen, J. Macromol. Sci. Part A **51**, 378 (2014)
8. A. Benvidi, M.D. Tezerjani, A.D. Firouzabadi, M. Mazloum-Ardakani, S.M. Moshtaghioun, J. Iran. Chem. Soc. **13**, 2135 (2016)
9. M.P. More, M.D. Patil, A.P. Pandey, P.O. Patil, P.K. Deshmukh, Artif Cells Nanomed Biotechnol **44**(1), 12–19 (2016)
10. T. Kavitha, A.I. Gopalan, K.P. Lee, S.Y. Park, Carbon **50**, 2994 (2012)
11. H. Mahdavi, O. Rahmani, A.R. Shahverdi, J. Iran. Chem. Soc. **14**, 37 (2017)
12. S. Chen, L. Bao, E. Ou, C. Peng, W. Wang, W. Xu, Nanoscale **7**, 19673 (2015)
13. N. Peimyoo, J. Li, J. Shang, X. Shen, C. Qiu, L. Xie, W. Huang, T. Yu, ACS Nano **6**, 8878 (2012)
14. S. Omidi, A. Kakanejadifard, F. Azarbani, J. Mol. Liq. **242**, 812 (2017)
15. E. Margapoti, P. Strobel, M.M. Asmar, M. Seifert, J. Li, M. Sachsenhauser, O.Z. Ceylan, C.A. Palma, J.V. Barth, J.A. Garrido, Nano Lett. **14**, 6823 (2014)
16. R. Devi, G. Prabhavathi, R. Yamuna, S. Ramakrishnan, N.K. Kothurkar, J. Chem. Sci. **126**, 75 (2014)
17. X. Zhang, Y. Feng, P. Lv, Y. Shen, W. Feng, Langmuir **26**, 18508 (2010)
18. F. Zhang, J. Wu, D. Kang, H. Zhang, J. Biomater. Sci. Polym. Ed. **24**, 1410 (2013)
19. H. Wang, M. Cheng, J. Hu, C. Wang, S. Xu, C.C. Han, ACS Appl. Mater. Interfaces. **5**, 11014 (2013)
20. Y.A. Son, G. Sun, J. Appl. Polym. Sci. **90**, 2194 (2003)
21. S. Ishikawa, Y. Matsumura, F. Yoshizako, T. Tsuchido, J. Appl. Microbiol. **92**, 261 (2002)
22. K. Hegstad, S. Langsrud, B.T. Lunestad, A.A. Scheie, M. Sunde, S.P. Yazdankhah, Microb. Drug Res. **16**, 91 (2010)
23. A. Kakanejadifard, F. Azarbani, A. Zabardasti, S. Kakanejadifard, M. Ghasemian, F. Esna-ashari, S. Omidi, S. Shirali, M. Rafieefar, Dyes Pigm. **97**, 215 (2013)

24. D.C. Marcano, D.V. Kosynkin, J.M. Berlin, A. Sinitskii, Z. Sun, A. Slesarev, L.B. Alemany, W. Lu, J.M. Tour, ACS Nano **4**, 4806 (2010)
25. B. Xue, J. Zhu, N. Liu, Y. Li, Catal. Commun. **64**, 105 (2015)
26. N.H. Kim, T. Kuila, J.H. Lee, J. Mater. Chem. A **1**, 1349 (2013)
27. S. Liu, T.H. Zeng, M. Hofmann, E. Burcombe, J. Wei, R. Jiang, J. Kong, Y. Chen, ACS Nano **5**, 6971 (2011)
28. V.K. Sarin, S. B. Kent. J. P. Tam, R. B. Merrifield. Anal. Biochem. **117**, 147 (1981)
29. Y. Xu, H. Bai, G. Lu, C. Li, G. Shi, J. Am. Chem. Soc. **130**, 5856 (2008)
30. G. Venugopal, K. Krishnamoorthy, R. Mohan, S.-J. Kim, Mater. Chem. Phys. **132**, 29 (2012)
31. D. Li, M.B. Müller, S. Gilje, R.B. Kaner, G.G. Wallace, Nat. Nanotechnol. **3**, 101 (2008)
32. M. Odabaşoğlu, Ç. Albayrak, R. Özkanca, F.Z. Aykan, P. Lonecke, J. Mol. Struct. **840**, 71 (2007)
33. H. Dinçalp, F. Toker, I. Durucasu, N. Avcıbaşı, S. Icli, Dyes Pigments **75**, 11 (2007)
34. O. Akhavan, E. Ghaderi, ACS Nano **4**, 5731 (2010)
35. W. Hu, C. Peng, W. Luo, M. Lv, X. Li, D. Li, Q. Huang, C. Huang, ACS Nano **4**, 4317 (2010)
36. C.J. Ioannou, G.W. Hanlon, S.P. Denyer, Antimicrob. Agents Chemother. **51**, 296 (2007)